metals

MDPI

Article

Design and Development of Complex Phase Steels with Improved Combination of Strength and Stretch-Flangeability

Alexis Graux [1], Sophie Cazottes [1,*], David De Castro [2], David San-Martín [2], Carlos Capdevila [2], Jose Maria Cabrera [3], Sílvia Molas [4], Sebastian Schreiber [5], Djordje Mirković [6], Frédéric Danoix [7], Damien Fabrègue [1] and Michel Perez [1]

1 Univ. Lyon, INSA Lyon, MATEIS, UMR CNRS 5510, F-69621 Villeurbanne, France; alexis.graux@insa-lyon.fr (A.G.); damien.fabregue@insa-lyon.fr (D.F.); michel.perez@insa-lyon.fr (M.P.)
2 Materalia Research Group, Centro Nacional de Investigaciones Metalúrgicas (CENIM-CSIC), Avda Gregorio del Amo 8, E-28040 Madrid, Spain; david.decastro@cenim.csic.es (D.D.C.); dsm@cenim.csic.es (D.S.-M.); ccm@cenim.csic.es (C.C.)
3 Polytechnic University of Catalonia, EEBE, c/Eduard Maristany 10-14, 08019 Barcelona, Spain; jose.maria.cabrera@upc.edu
4 Eurecat, Centre Tecnològic de Catalunya, Plaça de la Ciència 2, 08243 Manresa, Spain; silvia.molas@eurecat.org
5 Thyssenkrupp Steel Europe AG, Kaiser-Wilhelm-Straße 100, 47166 Duisburg, Germany; sebastian.schreiber2@thyssenkrupp.com
6 Salzgitter Mannesmann Forschung GmbH, Eisenhüttenstraße 99, 38239 Salzgitter, Germany; d.mirkovic@sz.szmf.de
7 Normandie Univ, UNIROUEN, INSA Rouen, CNRS, Groupe de Physique des Matériaux, 76000 Rouen, France; frederic.danoix@univ-rouen.fr
* Correspondence: sophie.cazottes@insa-lyon.fr; Tel.: +33-4-7243-8245

Received: 28 May 2020; Accepted: 18 June 2020; Published: 20 June 2020

Abstract: This study presents the design and development of a hot-rolled bainitic steel, presenting a good combination of strength and stretch-flangeability, for automotive applications. Ti, Nb, and Mo were added in the steel composition in order to control austenite grain sizes, enhance precipitation hardening, and promote the formation of bainite. This study focuses on the effect of process parameters on final microstructures and mechanical properties. These parameters are the finishing rolling temperature, which conditions the austenite microstructure before its decomposition, and the coiling temperature, which conditions the nature and morphology of the ferritic phases transformed. A preliminary study allowed to determine the austenite grain growth behavior during reheating, the recrystallization kinetics, and the continuous cooling transformation curves of the studied steel. Then, a first set of parameters was tested at a semi-industrial scale, which confirmed that the best elongation properties were obtained for homogeneous bainitic lath/granular microstructures, that can be produced by choosing a coiling temperature of 500 °C. When choosing those parameters for the final industrial trial, the microstructure obtained consisted of a homogeneous lath/granular bainite mixture that presented a Ultimate Tensile Strength of 830 MPa and a Hole Expansion Ratio exceeding 70%.

Keywords: metallurgy; complex phase steels; microalloyed steels; hot rolling; stretch-flangeability

1. Introduction

Over the last 20 years, car designers have been facing increasing challenges concerning passenger safety, vehicle performance, and fuel economy. More specifically, two demands have raised, leading to

the development by steelmakers of higher strength steel grades named Advanced High Strength Steels (AHSS). First, increasing steel strength allows to reduce the total weight of the car, therefore contributing to reduce CO_2 emissions. Second, for safety issues, increasing both yield and ultimate tensile strengths leads to enhanced crash performances. However, increasing strength generally lowers formability properties such as drawing, stretching, stretch flanging, or bending. Numerous chassis parts of the cars present complex shapes, and are manufactured by cold forming operations from steel plates, which requires good stretch-flangeability. The stretch-flangeability is indicative of the formability of the edges, and is usually evaluated by the hole expansion test [1]. It is related to the local ductility of the material, which can be quite different from the "global" ductility measured from a conventional tensile test. To improve the local ductility, it is important to limit the differences in hardness between phases present in the material, or to favor single phase microstructures.

Recently, a large effort has been made to develop steels reaching a good compromise of strength and stretch-flangeability. Three main strategies can be distinguished [2]: (i) ferritic steels reinforced by nanometer-sized precipitates [3,4]; (ii) reducing the hardness differences between martensite and ferrite in Dual Phase (DP) steels, either by reducing the hardness of martensite [5,6], or by increasing the one of ferrite [7,8]; and (iii) Complex Phase (CP) steels, which mainly present bainitic microstructures. The concept of CP steels initially emerged from the original idea of replacing martensite by bainite in DP steels [9]. CP steels present superior stretch-flangeability than DP steels with similar levels of tensile strength, which can be explained by their rather homogeneous microstructures [2].

As explained by Bhadeshia [10] (p. 367), a successful strategy to promote bainitic transformation is to use low carbon steels with additions of boron or molybdenum. Keeping a low carbon content avoid increasing the hardenability drastically, which would lead to the formation of martensite. Addition of B or Mo suppresses allotriomorphic ferrite formation, and promote the formation of bainite [11–14]. Ti, Nb, and V are added for their ability to form nanosized carbides, nitrides, or carbonitrides that are useful for precipitation hardening [15]. Moreover, those precipitates play an important role for austenite grain growth control, by limiting the grain boundaries motion [16].

The hot rolling process of bainitic steels is summarized in Figure 1. In hot rolling steel plants, the first step of the manufacturing process of steel sheets consists in a reheating stage, to ensure that the slab is ductile enough to be hot rolled. During this reheating, the steel is brought to a fully austenitic state. In the case of microalloyed steels, reheating ensures that primary coarse precipitates are dissolved before hot rolling, to optimize the effects of microalloying additions. After the reheating stage comes the proper hot rolling, which aims at reducing the slab thickness to get the targeted thickness of the final steel sheet. Hot rolling is divided in two stages, referred as roughing and finishing. The choice of deformation temperatures, of applied strain levels and strain rates, as well as the time between each deformation pass (interpass time) will have an influence on the phase transformation of the steel and therefore on its microstructure. The process ends with accelerated cooling on a run-out table, followed by coiling. The final microstructure will be highly influenced by the choice of the applied cooling rate and coiling temperature.

This work presents the design and development of a bainitic steel exhibiting a good compromise between strength and stretch-flangeability. The whole approach is shown, from the lab scale study of the chosen grade with the determination of Recrystallization-Precipitation-Time-Temperatures (RPTT) and the continuous cooling transformation (CCT) RPTT curves, to the industrial scale with the final microstructures and mechanical properties.

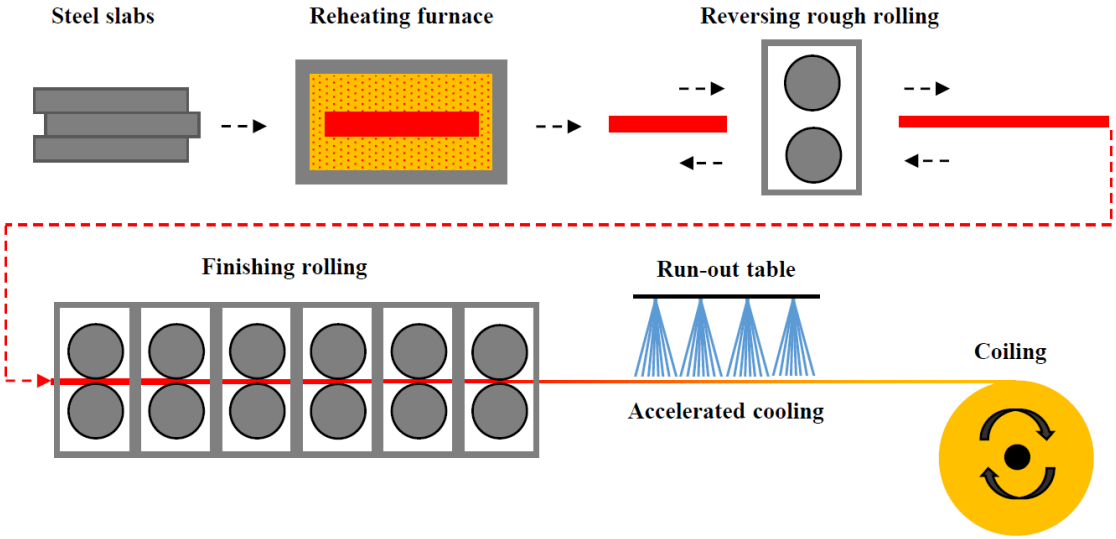

Figure 1. Schematic representation of the elaboration process of a bainitic steel sheet.

2. Preliminary Investigations

Preliminary investigations were first carried out, in order to gather critical information about austenite grain growth, recrystallization, precipitation, and phase transformation behavior of the chosen grade. Ti and Nb are added for their ability to form precipitates that control the austenite grain size at high temperature and enhance precipitation hardening after phase transformation, while Mo is added to promote the formation of bainite. The target composition is presented in Table 1. An ingot of approximate dimensions 140 × 150 × 50 mm^3 was produced by vacuum induction. After homogenization at 1200 °C for 2 h and hot rolling, a plate of 450 × 150 × 15 mm^3 was obtained. Table 1 provides the composition of the resulting alloy, measured by Induced Coupled Plasma-Mass Spectroscopy (ICP-MS).

Table 1. Bulk composition of the steel used for preliminary investigations (Lab scale), for pilot plant trials, and for industrial trials, determined by ICP-MS.

Element (wt%)	C	Mn	Si	Ti	Nb	V	Mo	Al	Cr	N
Target	0.06	1.9	0.5	0.1	0.04	0	0.2	0.05	0	0.005
Lab-scale	0.062	1.91	0.50	0.085	0.039	0.002	0.212	0.065	0.013	0.006
Pilot Plant trials	0.062	1.90	0.50	0.097	0.041	<0.001	0.208	0.053	0.093	0.0039
Industrial slabs	0.061	1.91	0.50	0.1	0.040	0.008	0.191	0.067	0.034	0.005

2.1. Selection of Reheating Temperature

The evolution of austenite grain growth and precipitation state during isothermal treatments were thoroughly investigated in a recently-published study [17]. A Bähr 805 DIL dilatometer was used to perform heat treatments consisting of a 5 °C s^{-1} ramp, followed by a 10 min holding at the reheating temperature and controlled cooling. For each heat treatments, austenite grain boundaries were revealed using thermal etching [18]. For isothermal annealing temperatures ranging from 900 °C to 1250 °C, the average austenite grain diameter increases from 10 µm to 400 µm. Graux et al. [17] showed that three types of precipitates are present in the alloys in the initial state: (Ti,Nb)C, $Ti_4C_2S_2$, and TiN precipitates. (Ti,Nb)C precipitates were the most frequently observed precipitates, and exhibit a mean diameter around 60 nm. They are the one controlling the austenite growth during soaking, as they exert a pinning pressure on austenite grain boundaries.

This former study allowed to select a temperature of 1250 °C for the reheating step of the hot rolling process and for all of the following investigations. Such high reheating temperature ensures a complete dissolution of the initial (Ti,Nb)C population controlling grain growth [17], which allows to fully benefit from microalloying additions in the next steps of the process. Although large austenite grains are obtained when reheating at 1250 °C, recrystallization could refine austenite grains during hot rolling.

2.2. Austenite Recrystallization Kinetics and Strain-Induced Precipitation

Afterwards, the microstructural evolutions of austenite after hot compression were investigated using stress relaxation in compression mode. Stress relaxation tests start with a reheating treatment of 10 min at 1250 °C. The sample is subsequently cooled down to the deformation temperature with a 5 °C s^{-1} cooling rate and held 30 s for homogenization before compression. After compression, the anvils remain fixed in their positions and hold the sample during a certain time period while recording the evolution of stress with time.

When both temperature and driving force are high enough, the recrystallization can be detected (Figure 2a). The curves were then processed following the method described in [19]. The beginning of the curve can be accurately described by a straight line ($\sigma_1 - \alpha_1 \cdot \log(t)$), corresponding to the recovery/creep behavior of the strained material. Then, the curve typically exhibits a sharp drop that is related to the rapid softening induced by the recrystallization process. The end of the curve also follows a linear trend, that corresponds mainly to the grain growth behavior of the recrystallized material ($\sigma_2 - \alpha_2 \cdot \log(t)$). Assuming that a partially recrystallized material consists of a mixture of two phases (work-hardened austenite and fully recrystallized austenite), a simple mixture rule is applied. Thus, the instantaneous value of stress is derived through the following equation: $\sigma = (1 - X) \cdot (\sigma_1 - \alpha_1 \cdot \log(t)) + X \cdot (\sigma_2 - \alpha_2 \cdot \log(t))$ where X is the recrystallized fraction. Therefore,

$$X = \frac{\sigma_1 - \alpha_1 \cdot \log(t) - \sigma}{(\sigma_1 - \sigma - 2) - (\alpha_1 - \alpha_2) \cdot \log(t)} \quad (1)$$

At lower temperatures or for insufficient driving forces, there is no recrystallization (Figure 2b), and a softening is observed, due to the recovery of the strained austenite. When precipitation occurs, a temporary increase in stress can be observed [20]. The beginning and end of the precipitation process are detected thanks to the deviation from the linear behavior.

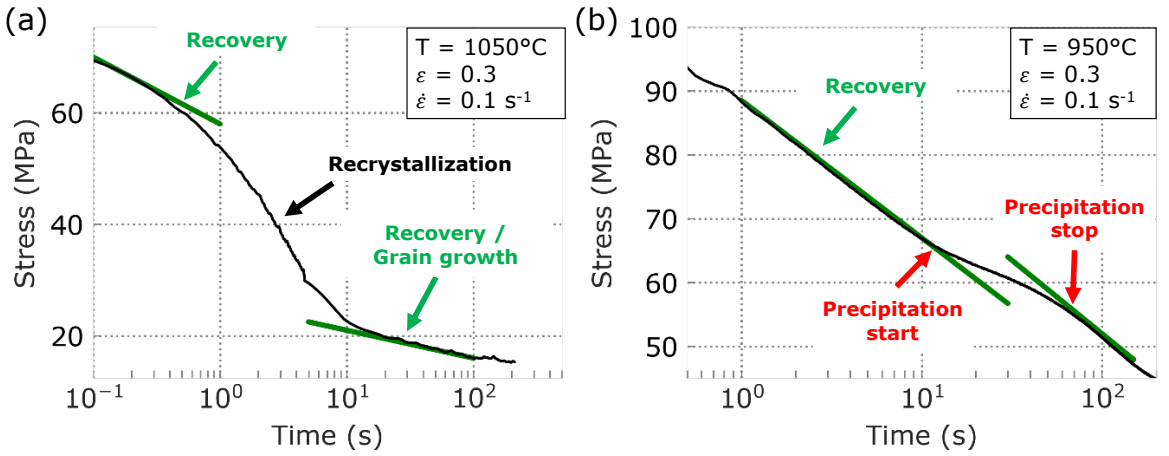

Figure 2. Illustration of the stress relaxation curves obtained at (**a**) 1050 °C and (**b**) 950 °C for $\epsilon = 0.3$ and $\dot{\epsilon} = 0.1\,s^{-1}$.

In this study, stress relaxations tests were conducted in compression mode, either using a Gleeble 3500 thermo-mechanical simulator on cylindrical samples of 12 mm length and 8 mm diameter or using

a Bähr 805 DIL dilatometer on samples of 10 mm length and 5 mm diameter. Two different strains (0.1 and 0.3) were tested and the temperatures ranged from 900 °C to 1100 °C. Because it is not suited for long time heat treatments, the Gleeble was dedicated to high temperatures (1000 ≤ T ≤ 1100 °C), to study static recrystallization. Recrystallization kinetics are known to depend on temperature, strain, but also on strain rate [21]. Therefore, two different strain rates (0.1 and 5 s^{-1}) were applied. For lower temperatures (T ≤ 1000 °C), the dilatometer was used to conduct the same stress relaxation tests, mainly to study strain-induced precipitation. As precipitation kinetics are much less sensitive to strain rates, these phenomena were studied using only one strain rate of 0.1 s^{-1}. These tests were performed using the Bähr 805 DIL dilatometer, presenting a higher sensitivity, which is needed to detect strain-induced precipitation on stress relaxation curves.

The stress relaxation tests performed allowed the reconstruction of complete Recrystallization-Precipitation-Time-Temperature (RPTT) diagrams, shown in Figure 3. An applied strain of 0.1 (Figure 3a) provides enough nucleation sites for the precipitation process to occur, so that precipitation is detected between 900 and 1000 °C. Above 1000 °C, no sign of recrystallization was detected, stress relaxation curves ($\sigma = f(\log t)$) exhibiting a linear decrease behavior due to recovery. When a larger deformation of $\varepsilon = 0.3$ is applied (Figure 3b), recrystallization is observed above 1000 °C, and precipitation at 950 and 900 °C. The increase in strain rate leads to an acceleration of the recrystallization kinetics. This is due to the fact that when higher strain rates are applied, higher stress values are reached during compression, leading to higher dislocation densities and driving energy for recrystallization.

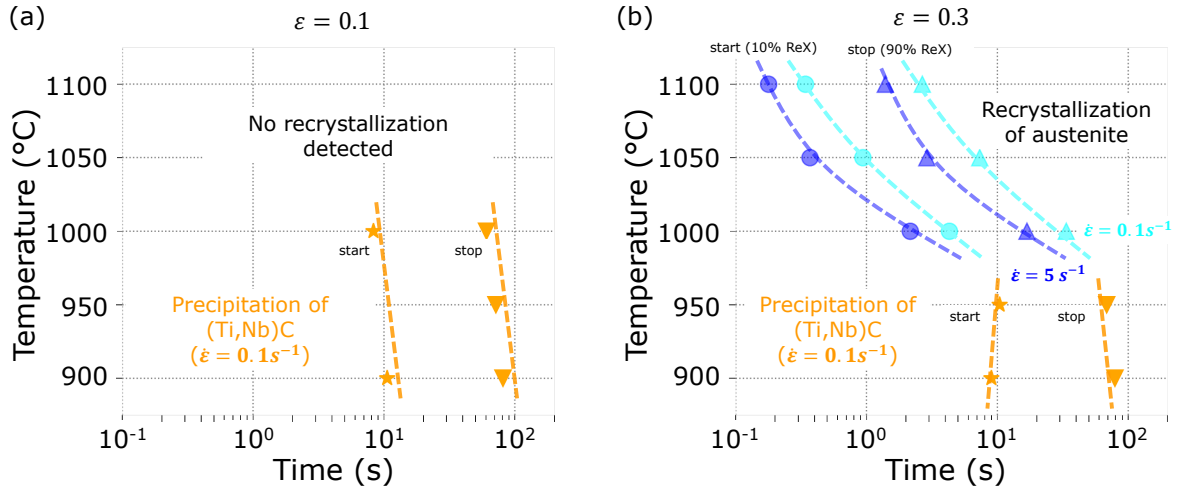

Figure 3. (**a**,**b**) Recrystallization-Precipitation-Time-Temperature (RPTT) diagram determined by stress relaxation method.

2.3. Continuous Cooling Phase Transformation

Continuous cooling experiments were performed using a Bähr 805 DIL dilatometer on samples of 10 mm length and 5 mm diameter. After a reheating treatment of 10 min at 1250 °C, the specimens were continuously cooled down to room temperatures at rates of 0.05, 1, 5, 10, and 25 °C s^{-1} (Figure 4a). In order to study the effect of austenite deformation on phase transformation, a second thermal cycle was applied (Figure 4b). After reheating, the samples were cooled down to 950 °C, held for 30 s, deformed to $\varepsilon = 0.3$ at a rate of 10 s^{-1}, and subsequently cooled down to room temperature at rates of 0.05, 1, 5, 10 and 25 °C s^{-1}. According to the study of recrystallization presented in Section 2.2, this deformation pass is performed in the non-recrystallization domain and thus results in austenite pancaking. During continuous cooling, the longitudinal dilatation curves were used to determine the transformation temperatures. It allowed the construction of the corresponding continuous cooling transformation diagrams, either starting from undeformed austenite or from deformed

austenite. Heat-treated dilatometry samples were cut in halves and the resulting microstructures were characterized by optical and scanning electron microscopy. Vickers hardness measurements were also performed using a 10 kg load. Figure 5 shows the microstructures obtained after continuous cooling from both undeformed and deformed austenite.

The cooling rate range for which bainitic microstructures were obtained is wide. Polygonal ferrite was only observed at the slowest cooling rate (0.05 °C s^{-1}). Starting from 1 °C s^{-1}, fully bainitic microstructures were observed. When higher cooling rates are applied, the morphology of bainite gradually changed from mainly granular bainite to fully lath-like bainite/martensitic microstructures. M_S is theoretically equal to 456 °C according to the MAP STEEL MUCG83 program [22]. The martensite start temperature M_S was not clearly detected by dilatometry. However, a residual amount of martensite was observed after the microstructural characterization of the steel samples using SEM, specially after cooling at 25 °C s^{-1}. Therefore, the high hardness values measured for the highest cooling rates (10 and 25 °C s^{-1}) could be mostly attributed to the fine microstructure of the bainite, though a small additional contribution from the residual martensite cannot be fully discarded.

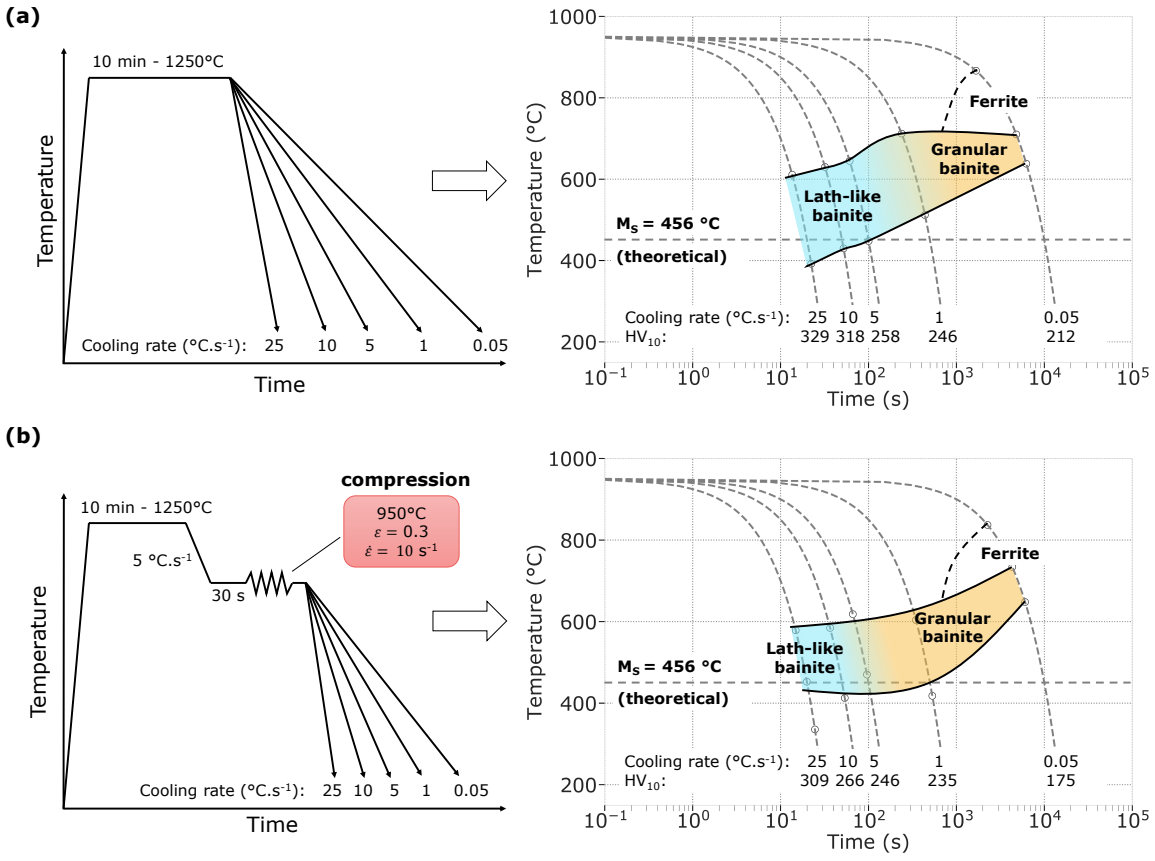

Figure 4. Thermal cycles applied and continuous cooling transformation diagrams with (**a**) undeformed austenite and (**b**) after austenite deformation at 950 °C with $\varepsilon = 0.3$ and $\dot{\varepsilon} = 10\,s^{-1}$.

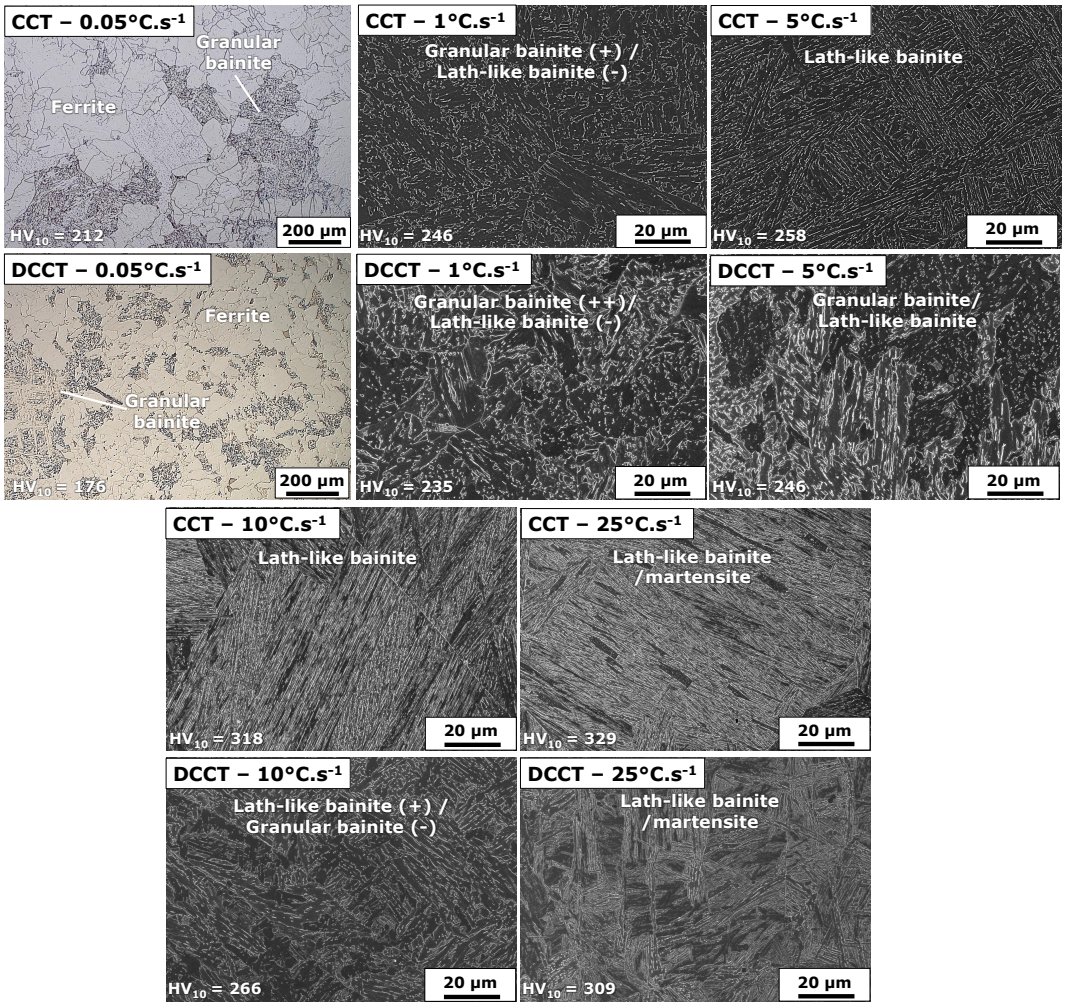

Figure 5. Microstructures resulting from continuous cooling experiments starting from undeformed austenite (CCT) and deformed austenite (DCCT). The (+) and (-) are indications of the major and minor phase constituent, respectively.

The deformation of austenite in the non-recrystallization region significantly affected the resulting microstructures. At a cooling rate of 0.05 °C s^{-1}, austenite deformation at 950 °C led to refined polygonal ferrite grains, as expected. The area fraction of granular bainite (≈30%) formed at 0.05 °C s^{-1} was however not affected by the deformation of austenite. Despite this apparent refinement of polygonal ferrite grains, a lower hardness was obtained when austenite was deformed, which can only be explained by different precipitation hardening levels. When austenite is undeformed, it is likely that no precipitation occurs in austenite before ferrite formation. Thus, a consequent precipitation strengthening should be obtained by interphase precipitation, as reported in previous studies on steels containing combined additions of Ti, Nb, and/or Mo [3,4,23–25]. On the contrary, due to the low cooling rate applied after austenite deformation, there should be plenty of time for precipitates to form in austenite, coherently with the RPTT diagram shown in Figure 3. Precipitates formed in austenite being coarser than the ones formed by interphase precipitation; those hypothesis could explain the lowered precipitation strengthening contribution for the sample submitted to austenite deformation.

Previous studies showed that austenite deformation has contradictory effects on bainite formation temperature [26,27]. In the present case, for high cooling rates (≥1 °C s^{-1}), austenite deformation lowered the bainite start transformation temperature, B_S. It also tended to increase the domain of granular bainite: for instance, granular bainite was observed at 5 °C s^{-1} when austenite was deformed whereas this type of bainite was not found when austenite was undeformed, which is coherent

with [28]. Another effect is the decreasing hardness of the lath-like microstructures, which is related to an apparent coarsening of the lath microstructures. Shorter and wider laths were obtained from pancaked austenite. This arises from the fact that dislocations hinder the growth of bainite laths, as reported by previous studies [29,30].

3. Pilot Plant Hot Rolling Trials

Different hot rolling strategies were tested on a laboratory hot rolling pilot plant, aiming at evaluating process conditions on microstructures and mechanical properties. Larger quantities of material were needed for hot rolling schemes. Thus, a second 100 kg ingot of approximate dimensions 120 × 140 × 600 mm^3 was produced by induction melting (Table 1). The 100 kg ingot was sectioned into coupons of 60 × 70 × 150 mm^3 intended to be hot rolled.

3.1. Definition of Hot-Rolling Strategies

Each hot rolling scheme entails five phases:

- Reheating at 1250 °C, ensuring a full dissolution of pre-existing (Ti,Nb)C precipitates (see Section 2.1).
- Rough rolling or roughing.
- Finish rolling or finishing.
- Accelerated cooling at 20–40 °C s^{-1} starting from the finishing rolling temperature (FRT) down to the simulated coiling temperature.
- Slow cooling down to room temperature once the coiling temperature is reached.

A reversing rolling mill was used to deform the plate, which resulted in rather large interpass times ranging from 11 to 18 s and deformation of about 30% for each pass. The initial thickness of the plate was 60 mm, and was reduced to 32 mm after the two roughing passes. A final thickness of 3.5 mm was reached after the five finishing passes. For such interpass times and deformation levels, the temperature of no-recrystallization (T_{NR}) is about 1000 °C according to the recrystallization kinetics determined by stress relaxation (Figure 3).

It was then decided to vary the temperature domain where deformation steps were applied with respect to the temperature of no-recrystallization, T_{NR}. Two distinct deformation schemes were defined:

- First, a recrystallization-controlled rolling strategy was tested (Figure 6a), with a finishing rolling temperature of 1050 °C. For this deformation scheme, all deformation passes were performed well above the temperature of no-recrystallization. In these conditions, austenite recrystallizes between each deformation pass, leading to grain refinement before accelerated cooling.
- Second, a more classical thermo-mechanical control process strategy was tested (Figure 6b). For this strategy, the two roughing passes are performed above 1050 °C leading to austenite grain refinement by recrystallization. After a waiting period of 30 s, the finishing stage was performed starting from 1050 °C, with a finishing rolling temperature of 880 °C. Therefore, most of the finishing passes were performed below T_{NR}, resulting in pancaked austenite.

After hot rolling, the plates were cooled down to the coiling temperature at a rate ranging from 20 to 40 °C s^{-1}. Finally, two different coiling temperatures were applied: 500 and 650 °C. After reaching the coiling temperature, the hot-rolled plates were stored into an insulated box in order to slowly cool them down to room temperature, with an estimated cooling rate of 0.5 °C min^{-1}, which is comparable to the cooling rates reached in industrial conditions after coiling. Thus, a total of four different hot rolling schemes were applied to generate different microstructures. Hot-rolled plates of 1050 × 160 × 3.5 mm^3 were finally obtained.

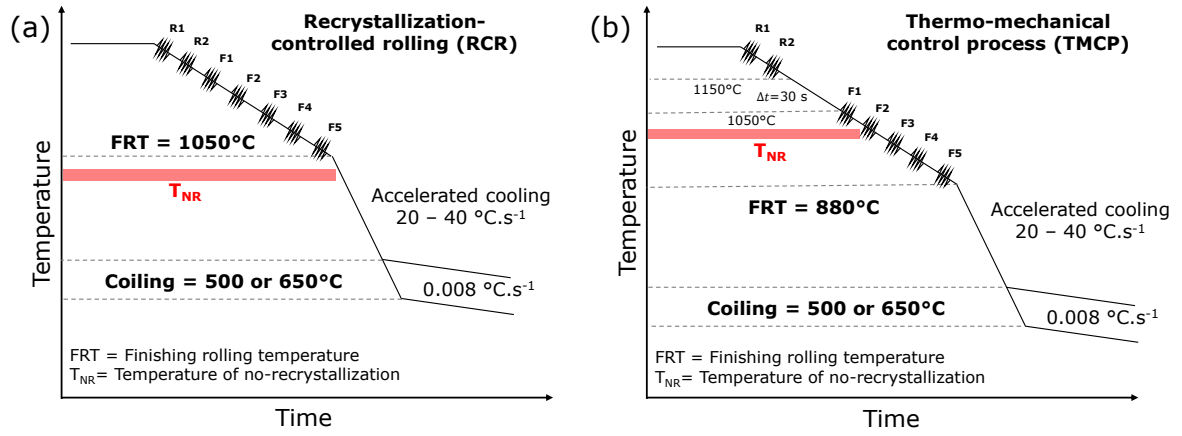

Figure 6. Schematic hot rolling schemes performed on pilot plant : (**a**) Recrystallization-controlled rolling (RCR) and (**b**) Thermo-Mechanical Control Process (TMCP). For each hot deformation scheme, two different coiling temperatures of 500 and 650 °C were applied, giving a total of four different hot rolling strategies.

3.2. Microstructures and Mechanical Properties

3.2.1. Methods

For microstructural characterization, parallelepiped samples were machined from the different hot-rolled plates. Observations were performed in the plan (RD, ND) at 1/4 thickness, where RD and ND stands for rolling and normal direction, respectively. After mechanical polishing, first with SiC paper and then down to 1 µm using diamond paste polishing, the samples were etched with nital (2 %). Scanning electron microscope observations using secondary electron (SE) were carried out with an accelerating voltage of 7 kV. For EBSD characterization, an additional polishing step was performed on a cloth soaked with a Struers OP-S colloidal suspension solution. Electron backscatter diffraction (EBSD) was carried out using a ZEISS Supra 55VP Scanning Electron Microscope operating at 20 kV, equipped with an Oxford Symmetry EBSD camera. The postprocessing analysis was performed on AZtec HKL Channel 5 software.

The mechanical properties of the plates obtained after hot rolling were characterized by tensile tests and hole expansion tests. The tensile tests were performed following the DIN EN ISO 6892-1 standard. The gauge length of the tensile samples are $55 \times 20 \times 3.5\,mm^3$. The tensile properties were evaluated according to three different orientations with respect to the rolling direction: at 0°, 45°, and 90°. As no clear anisotropy was observed in the sample, only the measurements made along the rolling directions are presented here. Two tensile samples were tested for each orientation, giving a total of 6 tensile samples per hot-rolling scheme. The values reported in the following are the average values (out of the six samples) for yield strength (YS), ultimate tensile strength (UTS), and total elongation.

Hole expansion tests were performed following the DIN EN ISO 16630 standard. Square specimens of $90 \times 90\,mm^2$ were machined from the plates. Holes with 10 mm initial diameter were punched in the center of the square samples of same thickness as the plates (3.5 mm to 4 mm) and expanded with a conical punch of diameter 40 mm and angle 60° until a crack at the edge of the expanding hole is observed. The hole expansion ratio (HER) was calculated through

$$HER(\%) = \frac{D_f - D_0}{D_0} \times 100 \quad (2)$$

where D_0 is the initial diameter and D_f is the final diameter. Three samples were tested for each hot rolling conditions. The standard error of the mean was calculated.

3.2.2. Microstructures

Figure 7 shows the microstructures obtained after the four different hot rolling strategies, characterized by means of SEM and EBSD. On EBSD maps, all grains are indexed as ferrite, and the phase nature identification is performed considering both the morphology and the grain/lath boundary misorientation, as explained by Zajac et al. [31]. The lath-like morphology of lath-bainite is usually accompanied with a high number of grain boundaries with a misorientation larger than 55°. Ferrite presents an equiaxed morphology with a random grain boundary misorientation, while the granular bainite rounded-shape morphology with grain boundary (GB) presents both small angle GB misorientation (<15°) as well as high angle GB misorientation (>15°). Low angle GB are plotted in red on the EBSD maps while GB larger than 15° are plotted in black. This representation allows a better visibility of the morphology of the grains.

All hot rolling strategies gave rise to microstructures mostly composed of (granular or lath-like) bainite. The main factor affecting the nature of the transformation products formed during the hot rolling process is the coiling temperature: coiling at 650 °C favors the formation of granular bainite (Figure 7a,b), whereas coiling at 500 °C favors the formation of (lath-like) upper bainite (Figure 7c,d). Hot deformation conditions, i.e., Recrystallization-Controlled Rolling (RCR) or Thermo-Mechanical Control Process (TMCP), also influences the nature and morphology of the observed phases. For the same coiling temperature of 650 °C, granular bainite was significantly refined when it formed from deformed austenite (TMCP-650 °C, see Figure 7b) compared to when it formed from recrystallized austenite (RCR-650 °C, see Figure 7a). Deformation in the non-recrystallization region also promoted the formation of slights amounts of deformed ferrite (TMCP-650 °C, which can be recognized as elongated grains formed along prior austenite grain boundaries in Figure 7b). In these conditions, the finishing rolling temperature is close to the austenite to ferrite transition equilibrium temperature, A_{e3}, equal to 860 °C according to Thermo-Calc [32]. Thus the slight amount of ferrite may have formed during the last rolling pass or right after it. The lath-like microstructures obtained after coiling at 500 °C were also influenced by austenite conditioning during hot deformation. RCR-500 °C (Figure 7c) scheme gave rise to a microstructure almost exclusively composed of lath-like bainite, with fine and long laths. When lath-like bainite is formed from deformed austenite (TMCP-500 °C, see Figure 7d), the resulting lath-like microstructure is coarser, presenting shorter and wider laths.

3.2.3. Mechanical Properties

Figure 8 presents the average tensile and hole expansion properties of the hot-rolled plates. As all hot-rolled plates presented bainitic microstructures, rather high levels of strength (UTS $\geq$ 800 MPa) were reached (Figure 8a), considering the low carbon contents of the studied steel. High YS/UTS ratios ($\geq$0.81) were also reached, which is a characteristic of complex phase steels. Figure 8b focuses on the ductility, evaluated by tensile tests (total elongation), and the stretch-flangeability, characterized by the HER. Plates coiled at 650 °C, with granular bainite microstructures, globally show higher ductility than the lath-like bainite plates coiled at 500 °C. The opposite tendency was observed for the HER, which is mainly governed by the local ductility of the plates. Plates coiled at 650 °C showed limited HER with a ceiling at 40%, whereas plates coiled at 500 °C showed enhanced stretch-flangeability, with HER ranging from 50 to 60%. As a consequence, the plates showing the best compromise between HER and strength are the ones coiled at a temperature of 500 °C, that contain mostly lath bainite. A better elongation is obtained with a lower FRT temperature (TMCP process) when pancaked austenite is formed before phase transformation.

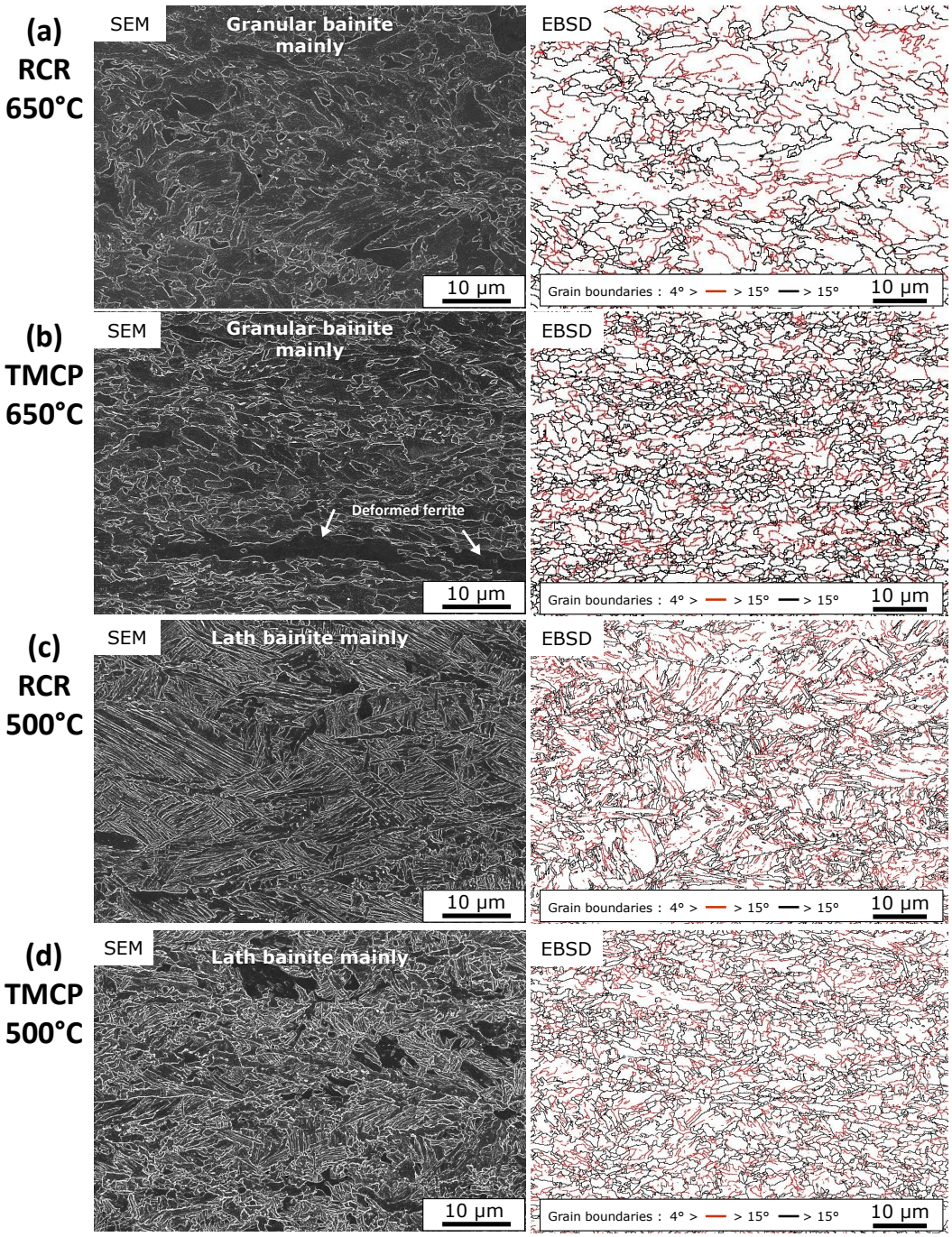

Figure 7. Microstructures of (**a**) RCR-650 °C, (**b**) TMCP-650 °C, (**c**) RCR-500 °C, and (**d**) TMCP-500 °C characterized by SEM and EBSD. Grain boundary maps showing grain boundaries between 4° and 15° in red and above 15° in black are displayed.

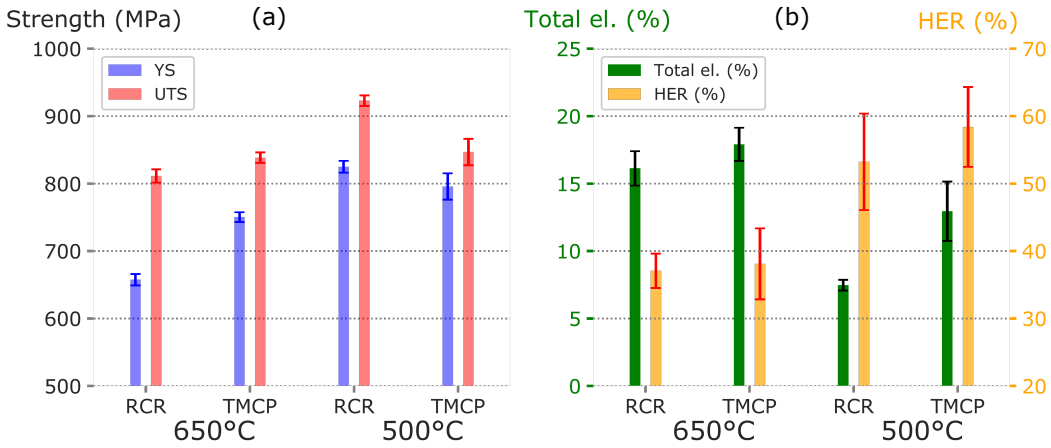

Figure 8. Mechanical properties of pilot plant hot-rolled plates, measured along the rolling direction. (**a**) Yield and ultimate tensile strengths. (**b**) Ductility properties : Total and uniform elongation determined by tensile tests, and hole expansion ratios.

4. Industrial Production Trial

The pilot plant hot rolling trials described in the previous section showed that lath-like bainitic microstructure obtained following a TMCP process with a coiling temperature of 500 °C provided the best compromise of strength and stretch-flangeability. The use of a FRT as high as possible is interesting industrially, as this allows lowering the forces applied during rolling, thus reducing the wear of the rolling mills and allowing a gain in productivity. The interpass times used during industrial trials were much smaller than the one used during pilot plant trials, which considerably reduced the time for recrystallization between two successive deformation passes. Thus, it was possible to increase significantly the FRT while still getting pancaked austenite before accelerated cooling. Therefore, the industrial trial was designed for a FRT of 990 °C and a coiling temperature of ~500 °C. The high FRT applied in this industrial trial is slighlty higher than the one choosen for the TMCP process presented for the pilot plant trial.

The inital slab, whose composition is presented in the Table 1, had an initial thickness of 250 mm. The roughing was performed between 1218 °C and 1126 °C, and the transfer bar thickness after this stage was 55 mm. Finishing was then conducted between 1126 °C and 991 °C, so that the final thickness was 3.8 mm. The coiling temperature achieved was 516 °C. This hot rolling scheme is close to the TMCP-500 °C one.

The microstructure of the industrial plate was characterised by means of SEM and EBSD, as shown in Figure 9. It consists of a mixture of lath and granular bainite, together with some tempered martensite (Figure 9b,c). This can be explained by the presence of retained (untransformed) austenite during coiling at 516 °C, that subsequently transforms into martensite during cooling. Some large TiN (2–4 µm) were also observed, and homogeneously distributed in the microstructure (Figure 9a). The strength obtained (UTS = 830 MPa) is comparable to the one obtained for TMCP-500 °C pilot plant trial, but a better hole expansion ratio (HER = 70%) is obtained. This result confirms that an homogeneous microstructure enhances the HER properties. The higher HER can be explained by the fact that a lower yield strength of approximately 700 MPa was obtained, compared to 800 MPa for the pilot plant one.

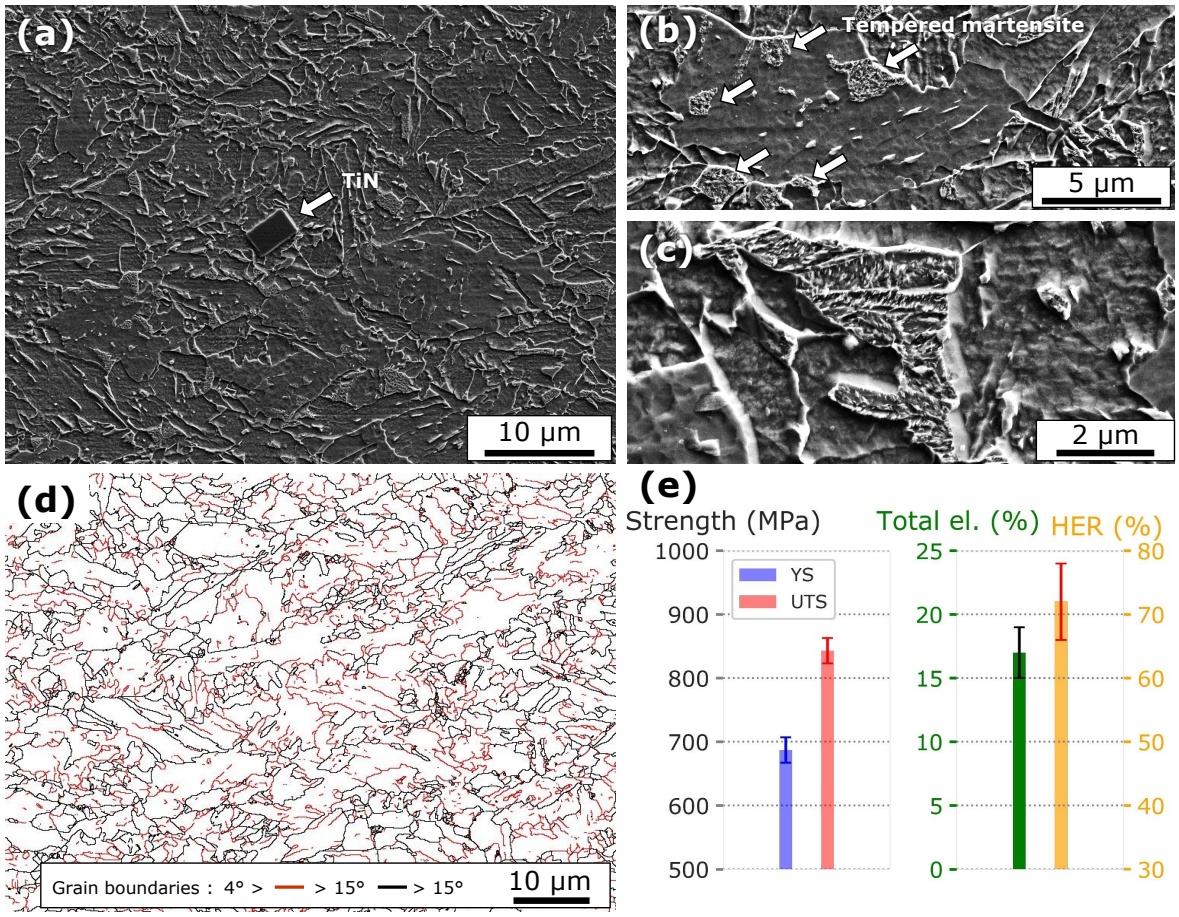

Figure 9. Microstructure of the industrial plate observed by SEM (**a**–**c**) and corresponding EBSD grain boundary map (**d**), consisting of a mixture of lath and granular bainite. Panel (**e**) shows the resulting tensile and hole expansion properties of this industrial plate.

5. Discussion

The steel composition studied in this work is particularly suitable for favoring bainite transformation. As demonstrated in part Section 2.3, bainitic microstructures were obtained for a wide range of cooling rates, even from deformed austenite. With cooling rates as low as 0.05 °C s^{-1}, a non-negligible fraction of austenite still transforms to granular bainite. The microstructures generated by pilot plant hot rolling trials also contain a very large proportion of bainite with, in the case TMCP schemes, small fractions of ferrite. The industrial production trial demonstrates the industrial feasibility of the steel design concept, even though the use of an industrial process induces significant changes in the final microstructure compared to pilot plant trials. In particular, the interpass times used during the industrial process are much shorter than those used in pilot plant trials. As a result, despite the high finishing rolling temperature used, austenite cannot be considered as fully recrystallized before accelerated cooling, consequently leading to an increased proportion of granular bainite in the final industrial steel microstructure. Moreover, due to the high finishing temperature, the short interpass time, the fast cooling, and the low coiling temperature chosen, the interphase precipitation is suppressed.

It was experimentally observed that microstructures consisting mainly of granular bainite led to lower hole expansion ratios than those mainly consisting of lath bainite. These observations are consistent with a recent study by Weißensteiner et al. [33] that reported that lath bainite microstructures exhibit higher tolerance against damage during the shearing of edges, and thus higher hole expansion ratios, than granular bainite ones. This may be due to the presence of large Martensite–Austenite (MA) islands in granular bainite (see Figure 10a). MA islands are formed during cooling to room

temperature, it is composed of small martensite laths and small blocks of retained austenite. As MA islands and bainite present different levels of hardness, stress concentration at interface between MA islands and bainite can induce crack nucleation. Lath bainite microstructures do not contain these large MA islands, as illustrated in Figure 10b. Thus, the formation of granular bainite should be avoided in order to achieve better HER.

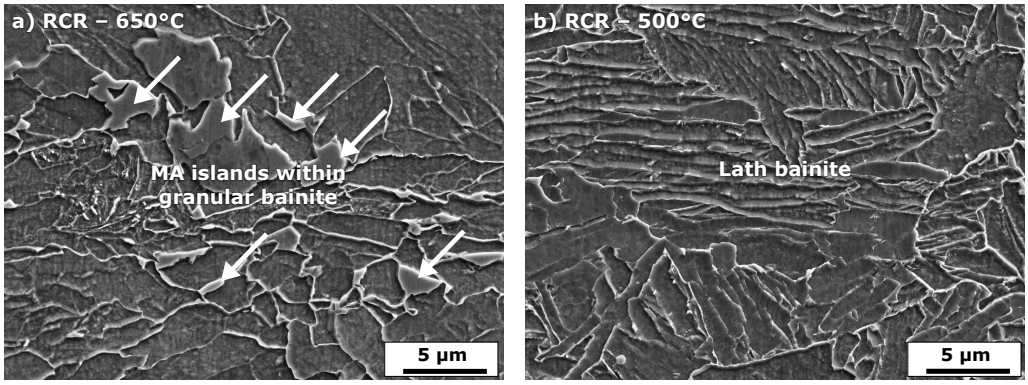

Figure 10. SEM observations of the microstructures of (**a**) RCR-650 °C and (**b**) RCR-500 °C hot-rolled plates. Nital etching.

Two recent studies [34,35] reported that large precipitates such as micrometric TiN or cementite can act as the primary source of void nucleation in complex phase steels, which deteriorates HER. Large TiN are also known to deteriorate the toughness [16]. The steel studied in this work contains a significant amount of micrometric TiN particles, an example of which is presented in Figure 9a. It is known that to avoid the formation of large TiN, the presence of TiN before solidification should be avoided by maintaining Ti and N contents below the solubility product of TiN at the solidus temperature [36]. Additionally, maintaining the Ti/N ratio below 3.42 reduces the coarsening rate of TiN during reheating [36,37]. In this study, the Ti/N ratio was considerably higher (Ti/N = 20 for the industrial trial), which explains the presence of coarse TiN in the microstructure. It would be interesting to try designing complex phase steels presenting lower amount of Ti to avoid forming large TiN. It should have a limited impact on the mechanical properties, as the best compromise HER and YS was achieved for process conditions that do not allow the precipitation of Ti and Nb.

6. Conclusions

The design and development of a bainitic steel grade presenting a combination of strength and stretch-flangeability for automotive application is presented.

After selecting a reheating temperature, experimental stress-relaxation curves were used to plot Recrystallization-Precipitation-Time-Temperature (RPTT) diagrams, which were useful for the determination of the temperature of non-recrystallization (T_{NR}) for the studied composition. Then, dilatometry tests, performed to estimate the effect of cooling rates on phase transformations are presented.

Those preliminary investigations allowed the selection of different hot rolling strategies that were applied in a pilot plant. Those strategies differ by the finishing rolling and coiling temperatures chosen, which strongly modify the microstructure and properties achieved. The study reveals that the coiling temperature was one of the most important parameters to adjust.

The best compromise between strength and stretch-flangeability was obtained for homogeneous microstructures developed after coiling at 500 °C. The choice of a low coiling temperature made it possible to transform austenite into lath bainite, and obtain a high final strength. The finishing rolling temperature was set to perform the last deformation passes below T_{NR} and thus induce austenite deformation prior to phase transformation. It is worth noting that, even with such low level of carbon,

a remarkable combination of properties by processing optimization was achieved, with an UTS value of 830 MPa together with a hole expansion ratio of 70%.

Author Contributions: Writing–original draft: A.G.; writing–review and editing A.G., S.C., D.F., M.P., and D.S.-M.; investigation, A.G., D.D.C., D.S.-M., and D.M.; supervision, C.C., J.M.C., S.M., S.S., D.M., A.G., D.S.-M., S.C., D.F., M.P., and F.D.; resources, D.M. and S.S.; funding acquisition, S.M., J.M.C., and C.C. All authors have read and agreed to the published version of the manuscript.

Funding: The authors gratefully acknowledge the funding received from the European Commission, Research Fund for Coal and Steel, under grant agreement 709803 (NANOFORM).

Acknowledgments: The authors gratefully acknowledge Florian Mercier (INSA Lyon) for his help and expertise with the Gleeble tests.

Conflicts of Interest: The authors declare no conflict of interest.

References

1. *ISO 16630:2017:Metallic Materials-Sheet and Strip-Hole Expanding Test*; ISO: Geneva, Switzerland, 2017.
2. Fonstein, N. Complex Phase Steels. In *Advanced High Strength Sheet Steels*; Springer: Berlin, Germany, 2015; pp. 241–258.
3. Funakawa, Y.; Shiozaki, T.; Tomita, K.; Yamamoto, T.; Maeda, E. Development of high strength hot-rolled sheet steel consisting of ferrite and nanometer-sized carbides. *ISIJ Int.* **2004**, *44*, 1945–1951. [CrossRef]
4. Kamibayashi, K.; Tanabe, Y.; Takemoto, Y.; Shimizu, I.; Senuma, T. Influence of Ti and Nb on the strength–ductility–hole expansion ratio balance of hot-rolled low-carbon high-strength steel sheets. *ISIJ Int.* **2012**, *52*, 151–157. [CrossRef]
5. Fang, X.; Fan, Z.; Ralph, B.; Evans, P.; Underhill, R. Effects of tempering temperature on tensile and hole expansion properties of a C-Mn steel. *J. Mater. Process. Technol.* **2003**, *132*, 215–218. [CrossRef]
6. Azuma, M.; Goutianos, S.; Hansen, N.; Winther, G.; Huang, X. Effect of hardness of martensite and ferrite on void formation in dual phase steel. *Mater. Sci. Technol.* **2012**, *28*, 1092–1100. [CrossRef]
7. Tsipouridis, P.; Werner, E.; Krempaszky, C.; Tragl, E. Formability of High Strength Dual-phase Steels. *Steel Res. Int.* **2006**, *77*, 654–667. [CrossRef]
8. Tsai, S.P.; Su, T.C.; Yang, J.R.; Chen, C.Y.; Wang, Y.T.; Huang, C.Y. Effect of Cr and Al additions on the development of interphase-precipitated carbides strengthened dual-phase Ti-bearing steels. *Mater. Des.* **2017**, *119*, 319–325. [CrossRef]
9. Sudo, M.; Hashimoto, S.I.; Kambe, S. Niobium bearing ferrite-bainite high strength hot-rolled sheet steel with improved formability. *Trans. Iron Steel Inst. Jpn.* **1983**, *23*, 303–311. [CrossRef]
10. Bhadeshia, H.K.D.H. *Bainite in Steels: Theory and Practice*, 3rd ed.; Maney Publishing: Leeds, UK, 2015.
11. Cizek, P.; Wynne, B.; Davies, C.; Muddle, B.C.; Hodgson, P.D. Effect of composition and austenite deformation on the transformation characteristics of low-carbon and ultralow-carbon microalloyed steels. *Metall. Mater. Trans. A* **2002**, *33*, 1331–1349. [CrossRef]
12. Zhao, M.C.; Yang, K.; Xiao, F.R.; Shan, Y.Y. Continuous cooling transformation of undeformed and deformed low carbon pipeline steels. *Mater. Sci. Eng. A* **2003**, *355*, 126–136. [CrossRef]
13. Kong, J.; Xie, C. Effect of molybdenum on continuous cooling bainite transformation of low-carbon microalloyed steel. *Mater. Des.* **2006**, *27*, 1169–1173. [CrossRef]
14. Hu, H.; Xu, G.; Wang, L.; Xue, Z.; Zhang, Y.; Liu, G. The effects of Nb and Mo addition on transformation and properties in low carbon bainitic steels. *Mater. Des.* **2015**, *84*, 95–99. [CrossRef]
15. Hu, J.; Du, L.X.; Wang, J.J. Effect of cooling procedure on microstructures and mechanical properties of hot-rolled Nb-Ti bainitic high strength steel. *Mater. Sci. Eng. A* **2012**, *554*, 79–85. [CrossRef]
16. Gladman, T. *The Physical Metallurgy of Microalloyed Steels*; Number 792 in Book / The Institute of Materials; Maney: London, UK, 2002.
17. Graux, A.; Cazottes, S.; De Castro, D.; San Martín, D.; Capdevila, C.; Cabrera, J.M.; Molas, S.; Schreiber, S.; Mirković, D.; Danoix, F.; et al. Precipitation and grain growth modelling in Ti-Nb microalloyed steels. *Materialia* **2019**, *5*, 100233. [CrossRef]
18. Garcıa de Andres, C.; Caballero, F.; Capdevila, C.; San Martin, D. Revealing austenite grain boundaries by thermal etching: advantages and disadvantages. *Mater. Charact.* **2002**, *49*, 121–127. [CrossRef]

19. Karjalainen, L.P. Stress relaxation method for investigation of softening kinetics in hot deformed steels. *Mater. Sci. Technol.* **1995**, *11*, 557–565. [CrossRef]
20. Liu, W.; Jonas, J. A stress relaxation method for following carbonitride precipitation in austenite at hot working temperatures. *Metall. Trans. A* **1988**, *19*, 1403–1413. [CrossRef]
21. Humphreys, F.J.; Rohrer, G.S.; Rollett, A.D. *Recrystallization and Related Annealing Phenomena*, 3rd ed.; Elsevier: Amsterdam, The Netherlands; Oxford, UK; Cambridge, MA, USA, 2017.
22. Peet, M.; Bhadeshia, H. Program MAP_STEEL_MUCG83. Materials Algorithms Project, 2006. Available online: http://www.msm.cam.ac.uk/map/steel/programs/mucg83.html (accessed on 6 June 2020).
23. Jha, G.; Haldar, A.; Bhaskar, M.; Venugopalan, T. Development of high strength hot-rolled steel sheet for wheel disc application. *Mater. Sci. Technol.* **2011**, *27*, 1131–1137. [CrossRef]
24. Jha, G.; Das, S.; Lodh, A.; Haldar, A. Development of hot-rolled steel sheet with 600 MPa UTS for automotive wheel application. *Mater. Sci. Eng. A* **2012**, *552*, 457–463. [CrossRef]
25. Wang, X.P.; Zhao, A.M.; Zhao, Z.Z.; Huang, Y.; Li, L.; He, Q. Mechanical properties and characteristics of nanometer-sized precipitates in hot-rolled low-carbon ferritic steel. *Int. J. Miner. Metall. Mater.* **2014**, *21*, 266–272. [CrossRef]
26. Nikravesh, M.; Naderi, M.; Akbari, G.H. Influence of hot plastic deformation and cooling rate on martensite and bainite start temperatures in 22MnB5 steel.*Mater. Sci. Eng. A* **2012**, *540*, 24–29. [CrossRef]
27. Hase, K.; Garcia-Mateo, C.; Bhadeshia, H. Bainite formation influenced by large stress. *Mater. Sci. Technol.* **2004**, *20*, 1499–1505. [CrossRef]
28. Jun, H.; Kang, J.; Seo, D.; Kang, K.; Park, C. Effects of deformation and boron on microstructure and continuous cooling transformation in low carbon HSLA steels. *Mater. Sci. Eng. A* **2006**, *422*, 157–162. [CrossRef]
29. Yamamoto, S.; Yokoyama, H.; Yamada, K.; Niikura, M. Effects of the austenite grain size and deformation in the unrecrystallized austenite region on bainite transformation behavior and microstructure. *ISIJ Int.* **1995**, *35*, 1020–1026. [CrossRef]
30. Fujiwara, K.; Okaguchi, S.; Ohtani, H. Effect of hot deformation on bainite structure in low carbon steels. *ISIJ Int.* **1995**, *35*, 1006–1012. [CrossRef]
31. Zajac, S.; Schwinn, V.; Tacke, K. Characterisation and Quantification of Complex Bainitic Microstructures in High and Ultra-High Strength Linepipe Steels. *Mater. Sci. Forum* **2005**, *500–501*, 387–394. [CrossRef]
32. Andersson, J.O.; Helander, T.; Höglund, L.; Shi, P.; Sundman, B. Thermo-Calc & DICTRA, computational tools for materials science. *Calphad* **2002**, *26*, 273–312. [CrossRef]
33. Weißensteiner, I.; Suppan, C.; Hebesberger, T.; Winkelhofer, F.; Clemens, H.; Maier-Kiener, V. Effect of Morphological Differences on the Cold Formability of an Isothermally Heat-Treated Advanced High-Strength Steel. *JOM* **2018**, *70*, 1567–1575. [CrossRef]
34. Pathak, N.; Butcher, C.; Worswick, M.; Bellhouse, E.; Gao, J. Damage evolution in complex-phase and dual-phase steels during edge stretching. *Materials* **2017**, *10*, 346. [CrossRef]
35. Karjalainen, A.; Kesti, V.; Vierelä, R.; Ylitolva, M.; Porter, D.; Kömi, J. *The Effect of Microstructure on the Sheared Edge Quality and Hole Expansion Ratio of Hot-Rolled 700 MPa Steel*; IOP Publishing: Bristol, UK, 2017; Volume 896, p. 012103.
36. Yan, W.; Shan, Y.; Yang, K. Effect of TiN inclusions on the impact toughness of low-carbon microalloyed steels. *Metall. Mater. Trans. A* **2006**, *37*, 2147–2158. [CrossRef]
37. Medina, S.F.; Chapa, M.; Valle, P.; Quispe, A.; Vega, M.I. Influence of Ti and N contents on austenite grain control and precipitate size in structural steels. *ISIJ Int.* **1999**, *39*, 930–936